


Article

3D Printed Chromophoric Sensors

Zachary Brounstein ^{1,2}, Jarrod Ronquillo ¹  and Andrea Labouriau ^{1,*}

¹ Los Alamos National Laboratory, Los Alamos, NM 87545, USA; zrbrounstein@lanl.gov (Z.B.); jarrodronquillo@lanl.gov (J.R.)

² Nanoscience and Microsystems Engineering, University of New Mexico, Albuquerque, NM 87131, USA

* Correspondence: andrea@lanl.gov

Abstract: Eight chromophoric indicators are incorporated into Sylgard 184 to develop sensors that are fabricated either by traditional methods such as casting or by more advanced manufacturing techniques such as 3D printing. The sensors exhibit specific color changes when exposed to acidic species, basic species, or elevated temperatures. Additionally, material properties are investigated to assess the chemical structure, Shore A Hardness, and thermal stability. Comparisons between the casted and 3D printed sensors show that the sensing devices fabricated with the advanced manufacturing technique are more efficient because the color changes are more easily detected.

Keywords: sensors; 3d printing; diw; Sylgard; chromophoric; indicators; halochromic; thermochromic



Citation: Brounstein, Z.; Ronquillo, J.; Labouriau, A. 3D Printed Chromophoric Sensors. *Chemosensors* **2021**, *9*, 317. <https://doi.org/10.3390/chemosensors9110317>

Academic Editor: Christos Kokkinos

Received: 19 October 2021

Accepted: 5 November 2021

Published: 9 November 2021

Publisher's Note: MDPI stays neutral with regard to jurisdictional claims in published maps and institutional affiliations.



Copyright: © 2021 by the authors. Licensee MDPI, Basel, Switzerland. This article is an open access article distributed under the terms and conditions of the Creative Commons Attribution (CC BY) license (<https://creativecommons.org/licenses/by/4.0/>).

1. Introduction

As an engineered and high-performance silicone material, Sylgard 184 is used for many specialized applications such as micro-separations and diffusion [1–5], triboelectric nanogenerators (TENG) [6–9], tissue engineering [10–13], and shape-memory and self-healing materials [14–17]. Many of the properties exhibited by Sylgard 184 (which may be referred to in literature as poly (dimethyl siloxane) (PDMS)) are due to the Si-O-Si bond, which gives flexibility to silicones, and to the ease of controlling the functional groups and side chains of siloxanes. Additionally, many new and enhanced characteristics can be imbued to Sylgard 184 by incorporating fillers and other polymers to create composite materials. Indeed, the facile ability to combine metals, ceramics, glasses, functionalized particles, and/or biomolecules into Sylgard 184 and develop distinct layers that can contain heterogeneous fillers makes it an incredibly versatile and popular polymeric system. Our team has previously worked on aspects of this, where composites were made using different types of Sylgard or siloxanes and fillers to alter the surface adhesion and thermomechanical properties [18,19].

One class of composites that has been studied and heavily developed is that of Sylgard 184 sensors. Indeed, Sylgard 184 is an ideal candidate for sensing applications because of its selective permeability to gases, optical transparency, chemical inertness, and ease of patterning via soft lithography, casting, and other techniques. As such, quite a bit of research has explored Sylgard 184 in active and passive sensors such as lab-on-a-chip devices for biosensing [20–22], mechanoresponsive devices, e.g., capacitive pressure (or tactile) sensors [23,24] and strain sensors [25,26], and environmental sensors that can detect changes in temperature [27,28], pH [29–31], relative humidity [32,33], and certain gas species [34,35]. In high-hazard occupations or areas where workers may be exposed to hazardous conditions, a device that produces an easy to see change can alert workers if a dangerous threat is immediately present. Such a sensor would need to have a long lifespan, function continuously and passively, and demonstrate an irreversible visual cue in order to protect people in situations with inherent risk.

Three hazards that could be present in high-risk occupational areas include elevated temperatures, acidic chemical species, or basic chemical species. If a visual cue was available, such as a color change in a sensor, this could help alert workers if one of these hazards

is immediately present. Compounds exist that do exhibit halochromic and thermochromic effects. Some of these include pure indicators such as thymol blue, bromothymol blue, phenolphthalein, methyl red, and methyl yellow as well as commercially available indicating paints. The pure indicators exhibit their halochromic effects through similar mechanisms, where protonation and deprotonation cause a macroscopic color change [36–38]. Thymol blue has been encapsulated in a siloxane matrix, where its surface area effects and sensitivity to pH was investigated [39]. Thymol blue has also been used to detect CO₂ via pH in a europium polymer composite film [40,41]. Bromothymol blue has been used with high density polythethylene (HDPE), ethylene-vinyl acetate (EVA), and silica to detect spoiled milk via pH changes [42] and combined with carbon nanotubes to detect epinephrine [43]. The well-known pH indicator phenolphthalein has been functionalized with formaldehyde and immobilized in diacetylcellulose to create an optical sensor [44] as well as electrospun with poly(acrylonitrile-co-vinyl acetate) (PAN) in N, N-dimethylformamide (DMF) to develop halochromic nanosensors [45]. Besides being halochromic, methyl red exhibits excellent humidity sensing capabilities and research groups have inkjet-printed composites of methyl red with graphene in-between inter-digital transducer (IDT) electrodes to develop highly sensitive devices [46,47]. Additionally, the transesterification reaction of tris(isopropyl)amine and methyl red-amidopropyltrimethoxysilane (MR-APTMS) results in a colorimetric sensor that can detect Hg²⁺ in the micromolar levels [48]. Methyl yellow has found many uses in various sensors and devices, where one notable application is in the detection of formaldehyde via pH changes [49–51]. These compounds, along with some commercial indicating paints, could be used in the facile fabrication of passive environmental sensors that can alert workers if certain hazards are immediately present.

In this work, Sylgard 184 was used as the encapsulating network for halochromic and thermochromic indicators. Passive environmental chromophoric sensors were created and their performance was assessed via high-temperature and liquid and vapor phase exposure to acidic and basic chemical species. Additionally, the composite sensors were enhanced by developing 3D printed Direct Ink Writing (DIW) formulations and subsequently printing devices with increased surface areas and porosity in order to create a better visual cue of any color change. Material properties of the sensors were investigated via solvent swelling, Shore A Hardness, and thermogravimetric analysis experiments.

2. Experimental

2.1. Materials

Dow SYLGARD™ 184 Silicone Elastomer was formulated from a base agent and curing agent, both of which were supplied by Ellsworth. Acid Detecting Paint and Base Detecting Paint, referred to in this study as acid paint and base paint, respectively, were both purchased from RAMCO Manufacturing Company. Non-Reversible Single-Change Indicating Thermal Paint 155 °C/311 °F, referred to in this study as thermal paint, was purchased from TIPTEMP. Thymol blue, bromothymol blue, phenolphthalein, methyl red, and methyl yellow were purchased from ACROS Organics. TS-720 CAB-O-SIL fumed silica was purchased from Cabot Corporation. The liquids such as HPLC-grade toluene, 1-propanol, hydrochloric acid, nitric acid, ammonium hydroxide, and sodium hydroxide were supplied by Thermo Fisher Scientific. Ultra-high purity nitrogen was supplied by Airgas. All chemicals were used as received.

2.2. Formulation Development

Eight chromophoric indicators were investigated in this study. Three indicators were in paint form: acid detecting paint; base detecting paint; and non-reversible single-change indicating thermal paint 155 °C. Throughout this study, these will be referred to as acid paint, base paint, and thermal paint, respectively. Acid paint changes color from yellow to red when its pH drops below 3. Base paint changes color from white to blue when its pH rises above 10. Thermal paint changes color from turquoise to green-gray when it is exposed to temperatures above 155 °C for ten continuous minutes. Five indicators were

in pure powder form: thymol blue; bromothymol blue; phenolphthalein; methyl red; and methyl yellow. The powders range in colors and can change acidic and basic solutions to varying hues depending on the pH of the solution, which are listed in Table 1.

Table 1. Solution pH and colors associated with the powder indicators in this study.

Indicator	Solution pH, Color	Solution pH, Color
Thymol blue [36]	<8, yellow	>9, blue
Bromothymol blue [38]	<6, yellow	>7, blue
Phenolphthalein [52]		>8, pink
Methyl red [52,53]	<4, red	>6, yellow
Methyl yellow [53]	<3, red	>4, yellow

A ratio of 10:1 *w/w* of base agent to curing agent was used to make Sylgard 184. Using a THINKY ARV-310 planetary mixer, the indicator and base agent were mixed for two minutes at 2000 rpm at a vacuum of 0.2 psi and then the curing agent was added using the same mixing settings. This resulting solution was then poured in molds and cured at 25 °C for one week. Although Sylgard 184 cures and can be used within two days, full mechanical properties are not reached until one week after mixing. When making the 3D printing formulations, PDMS-functionalized fumed silica was incorporated into the base/indicator slurry to create a non-Newtonian shear-thinning fluid that was suitable for DIW 3D printing. The proportions of the 3D printing formulations included 15 wt.% fumed silica.

Four different weight percents of the indicators were tested (0.5, 1, 5, and 10 wt.%) and almost all exhibited the property of being successful as a sensor at all proportions. Table 2 lists the notation for the passive environmental sensors used in this study along with their components.

Table 2. Notation of the passive environmental chromophoric sensors used in this study and their components.

Sample	Components		
tpS184	Sylgard 184	+	thermal paint
bpS184	Sylgard 184	+	base paint
apS184	Sylgard 184	+	acid paint
tbS184	Sylgard 184	+	thymol blue
bbS184	Sylgard 184	+	bromothymol blue
ppS184	Sylgard 184	+	phenolphthalein
mrS184	Sylgard 184	+	methyl red
myS184	Sylgard 184	+	methyl yellow

2.3. Material Characterization Techniques

While the chemistry of curing PDMS via the hydrosilylation reaction is well-known, if any of the bonds or functional groups of the indicators changed while in the Sylgard 184 composite, then the sensor may not function as designed. To ensure that the composites had their components intact, Fourier transform infrared (FTIR) spectroscopy was performed on the samples. A ThermoScientific Nicolet iS50 FT-IR instrument was used in Attenuated Total Reflection (ATR) mode with a diamond crystal reference and an average of 32 scans at a resolution of 4 cm⁻¹ between 4000–525 cm⁻¹. The stage was cleaned and a background spectrum was taken before each measurement.

Acid and base exposure experiments were performed as vapor and liquid phase tests. For the liquid phase tests, a single drop of each acid (hydrochloric acid and nitric acid, both at a pH of 0) or base (ammonium hydroxide at a pH of 12 and sodium hydroxide at a pH of 14) was placed on the surface of the samples. For the vapor phase tests, hydrochloric acid or ammonium hydroxide were placed in small open vials within a closed glass chamber along

with a pH strip on the sidewalls of the chamber and a composite halochromic sensor located in the middle. The acids and bases were tested with pH strips for the liquid and vapor phase tests to ensure that the experiments did not yield false negatives or false positives for the sensors. Changes in color for the liquid and vapor phase tests were documented with respect to time using a stopwatch. Elevated temperature exposure experiments were performed for the tpS184 samples in an oven at 160 °C. Enough tpS184 samples were placed in the oven so that they could be removed in 30 min intervals.

Chromophoric behavior was assessed by performing ultraviolet-visible (UV-Vis) spectrophotometry on pristine and exposed samples. UV-Vis spectrophotometry experiments were conducted on an AvaSpec-ULS2048CL-EVO detector and a grating of 300 lines/mm, which has a range spanning 200–1100 nm. Natural light was used as a light source and spectra were obtained with measurements using the same darkness reference.

Solvent swelling experiments were used to evaluate the crosslinking of the polymer network in each sample. The composite passive environmental sensors were swollen to equilibrium in toluene for 24 h at 25 °C. After being swollen, the samples were gently patted dry to remove residual toluene before recording the swollen mass. The samples were subsequently dried at 25 °C for 24 h and then at 70 °C for 48 h under vacuum. Percent loss from the solvent is reported as the difference between the initial mass and the vacuum dried mass. The network swelling is reported as the difference between the fully swollen mass and vacuum dried mass. Densities were evaluated by measuring the initial masses and volumes. Each sample was run in triplicate and standard deviation is reported as the error.

By using the density and solvent swelling data, crosslink density values for the polymer composites can be determined. The Flory-Rehner equation for a phantom network was applied because it models the PDMS and toluene system well [54,55]. The specific crosslink density ν_x , in units of moles of crosslinks per gram of material, is the reciprocal of the average molecular weight of the polymer between crosslinks M_c , which was derived in previous work [56]. It is a function of the polymer volume fraction φ_p , the Flory–Huggins polymer–solvent interaction parameter χ , the polymer density ρ_p (which is taken as the density of the composite), and the molar volume of the solvent $v_{m,s}$ (for toluene, this value is 106.2 mL/mol) (Equation (1)). The polymer volume fraction was calculated from the network swelling S and the densities of the polymer and solvent (Equation (2)). Many groups have studied the interaction between PDMS and toluene and proposed that the Flory–Huggins polymer–solvent interaction parameter can be modeled from the polymer volume fraction (Equation (3)) [57].

$$\nu_x = \frac{1}{M_c} = \frac{\ln(1 - \varphi_p) + \varphi_p + \chi\varphi_p^2}{-\frac{1}{2}v_{m,s}\rho_p\varphi_p^{\frac{1}{3}}} \quad (1)$$

$$\varphi_p = \left(1 + S\frac{\rho_p}{\rho_s}\right)^{-1} \quad (2)$$

$$\chi = 0.459 + 0.134\varphi_p + 0.590\varphi_p^2 \quad (3)$$

Each composite's resistance to indentation, or hardness, was assessed with a benchtop HPE II Zwick Roell Shore A durometer. Cylinders measuring 12 mm in height and 26 mm in diameter were used as durometry test samples. Each composite had three samples and two trials were conducted on each cylinder in different locations. Shore A Hardness values were averaged from these trials and the standard deviations are reported as the error.

To evaluate the thermal stability and decomposition of the composites, Thermogravimetric analysis (TGA) experiments were conducted using a TA Instrument TGA 550, Discovery Series. Samples weighing approximately 10 mg were subjected to a heating ramp of 10 °C/min until they reached 750 °C while in an inert nitrogen atmosphere flowing at 20 mL/min. The onset of thermal degradation, Td5%, is the temperature at which the residual mass is 95%. The decomposition temperature, TdMax, is the temperature at which

the derivative curve (DTGA) is a maximum. The final residual mass, *mf*, is the mass percent that remains after the TGA experiment has ended.

Chromophoric composite sensors for 3D printing were formulated for DIW. 3D printing was performed using a Hyrel 30M printer and EMO-25 printer head along with the Repetier software (all Hyrel products). A 250 μm nozzle was used with a travel rate of 2250 mm/min to extrude the material, which was programmed to have a flow rate of 150 pulses/ μL . Finished printed parts were 5 cm diameter disks comprising eight layers of a staggered face-centered tetragonal (FCT) geometry with a 500 μm spacing between the centers of two struts. The parts were cured at 25 $^{\circ}\text{C}$ for two days or at 150 $^{\circ}\text{C}$ for two hours.

Magnified top and cross-section views of the samples were taken using a confocal digital microscope (Keyence VHX-6000). Magnifications of 20 \times –150 \times were used to investigate the network of the resulting 3D printed pads. Measurement of the beams was obtained from the Keyence analysis software.

3. Results and Discussion

3.1. Sensor Performance

A top view of all the composite chromophoric sensors in this study is shown in Figure 1. The lowest and highest proportions of indicators (0.5 wt.% and 10 wt.%) were used in the figure to observe how the intensity of the initial colors could be distinguished.

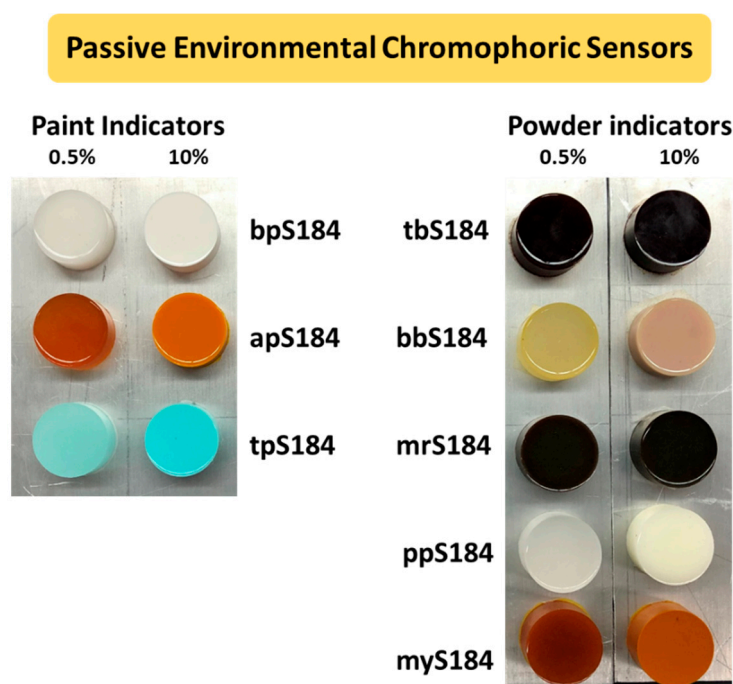


Figure 1. Pristine composite passive environmental chromophoric sensors separated by indicator weight percent (0.5 wt.% on the left and 10 wt.% on the right of each photo) and by the initial indicator form (paint-based on the left and powder-based on the right).

Using the four different proportions of indicators (0.5%, 1%, 5%, and 10% by mass), liquid and vapor phase tests were conducted on all the samples except for tpS184, in which case elevated temperature experiments were performed. Generally, cylinders measuring 12 mm in height and 26 mm in diameter were used, but flat films measuring between 1 to 2 mm in thickness were also investigated. It was found that if a sensor worked for the vapor phase tests, then they successfully worked in the liquid phase tests.

While the liquid phase tests produced a more obvious change, vapor exposure represents a more difficult hazard to identify and mitigate in occupational scenarios, therefore vapor phase tests were considered a better standard with which to compare the samples.

Pristine specimens were placed in a container with a vial of a volatile acidic or basic solution for three minutes. The associated color changes of the 0.5 wt.% sensors are shown in Figure 2 along with tpS184, which was subjected to 160 °C for 45 min. Within a few seconds, apS184 began changing from orange to red. After three minutes, tbS184 changed from dark green to reddish violet. Although the color change is obvious when in certain light, the pristine and exposed tbS184 are both dark and it can be difficult to distinguish between the two in low-light conditions. Going from beige-yellow to a mossy green, bbS184 began visibly changing first at the rim after two minutes then slowly spread to the rest of the sample. Another interesting phenomenon occurred to bbS184 samples a day after both liquid and vapor exposure, where the specimen changed from mossy green to bright yellow and red. This has been observed in multiple samples across varying proportions. Therefore, a temporal color change phenomenon is exhibited in bbS184, where immediate basic species exposure results in a change to a green hue and in the days after exposure results in a yellow and red hue (see Figure 3). Like the apS184 samples, within a few seconds the myS184 specimen began changing color, however the color change was to a much darker red. After 45 min in a 160 °C oven, the tpS184 samples changed from turquoise to greenish gray. Films with less than 5 wt.% thermal paint and that were 1 mm thick did not exhibit a blueish hue and thus the color changing properties were not discernable. Films with 5 wt.% thermal paint and between 1 and 2 mm thick showed a color change after 30 min. Therefore, thicker samples require more time for the thermal paint composite sensors to change color while also needing less indicator to be thermochromic. It should be noted that films made with the other indicators exhibited enough of a color change to be distinguishable from regular Sylgard 184 for all indicator concentrations and thus could be used as sensors. Another important observation was that the exposed samples remained in their altered colored state without any signs of reversing to their pristine condition, even after a year following exposure. Additionally, the sensors were able to perform as intended after a storage period after a year, where the pristine samples changed color once exposed. Thus, these composite sensors demonstrate an irreversibility and long lifespan that aids in their passive behavior.

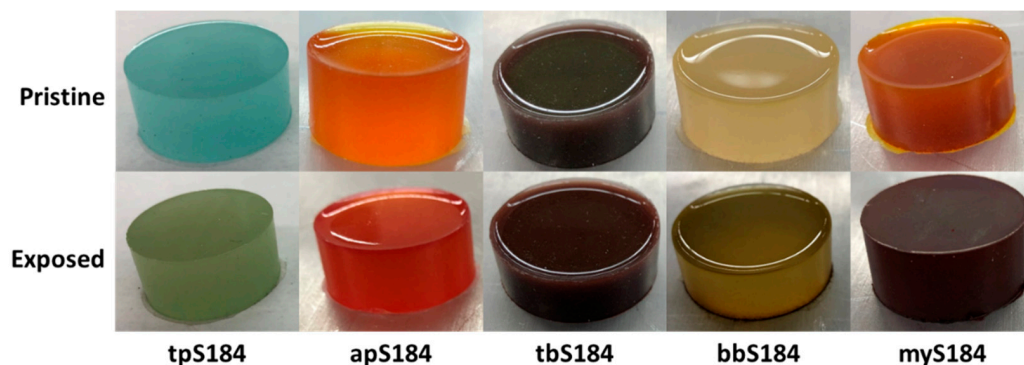


Figure 2. Comparison of the color changes between pristine and exposed composite chromophoric sensors (0.5 wt.%).

Three composites did not work for the vapor phase tests: bpS184; mrS184; and ppS184. Subjecting strong bases in the form of liquid droplets to the bpS184 samples also did not produce a color change. This indicates that bpS184 would not be applicable as a sensor for any of the concentrations. While mrS184 did not produce an observable color change during the vapor phase tests, an issue with the composite is that for all proportions made, mrS184 was too dark in hue to make accurate color comparisons. A similar phenomenon occurred with ppS184, except that the pristine coloring was light enough to discern that no color change transpired with vapor and liquid phase tests. To assess the color changes, ultraviolet-visible (UV-Vis) spectrophotometry was performed on the tpS184, apS184, tbS184, bbS184, myS184, and mrS184 samples. With a range spanning 200–1100 nm, UV-Vis spectroscopy provides a better determination on how the sensors

exhibited their chromophoric behavior. Comparing the pristine and exposed samples demonstrated obvious changes for each sensing device (see Figure 4) by way of shifting, adding, or subtracting peaks in a spectrum. Furthermore, the spectroscopy data validated that some samples may be difficult to distinguish between pristine and exposed states. This includes tbS184 and mrS184, where the biggest peaks show a slight shifting towards larger wavelengths (approximately 700 nm) and a subtraction of the peaks shorter than 640 nm, which is not as drastic a change as the other sensors. Thus, while all of these specimen exhibit some chromophoric property, making the tbS184 and mrS184 sensors as a solid device does not prove to be feasible for detecting a color change with the unaided eye.

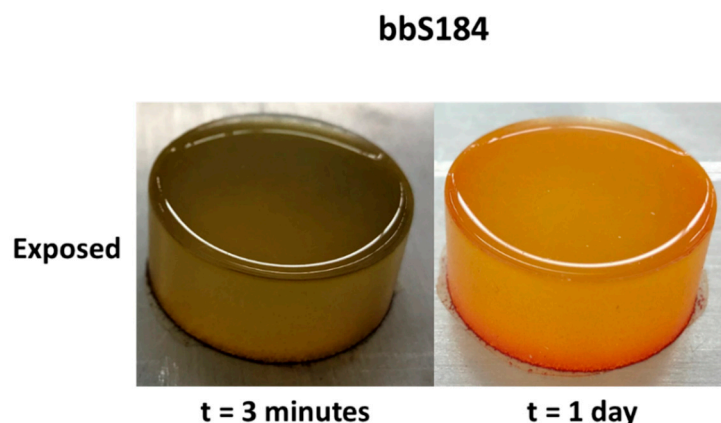


Figure 3. The temporal change of bbS184 one day after exposure.

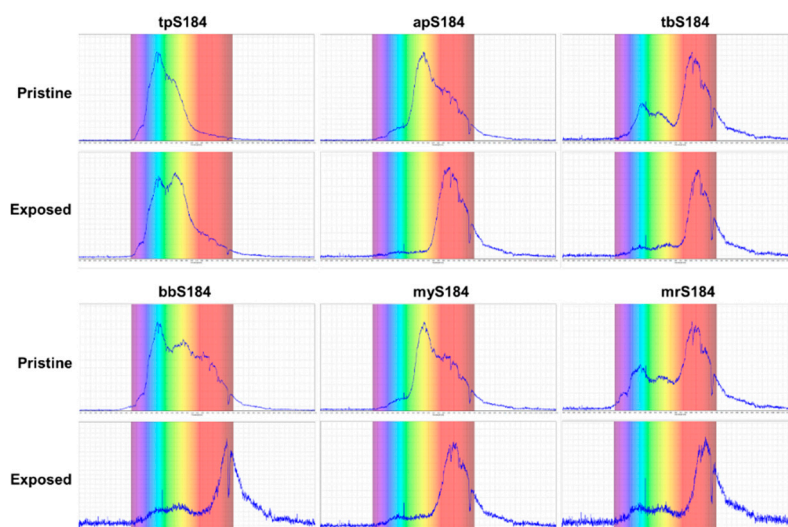


Figure 4. UV-Vis spectrophotometry data demonstrating the chromophoric behavior of the sensing devices.

Despite the vapor and liquid phase tests not changing the color of mrS184 samples dramatically enough to be able to distinguish the exposed from the pristine specimen to the naked eye, applying acidic solutions as droplets to the samples did reveal surface effects. The droplets were clear solutions when applied to mrS184 samples and quickly turned a dark yellow-orange hue. When the acidic solutions were wiped away, no visible markings were left on the samples, but the wipes retained a yellow-orange residue. This occurred with all proportions of mrS184. In a similar fashion, when a basic droplet was applied to ppS184 samples, the liquid changed from clear to bright pink (see Figure 5). And akin to mrS184, wiping away the liquid left no markings on the sample but a visible residue (bright pink) on the wipe. Thus, bpS184 exhibits no sensing properties while mrS184

and ppS184 exhibit surface sensing when in contact with liquid drops of acidic and basic species, respectively.

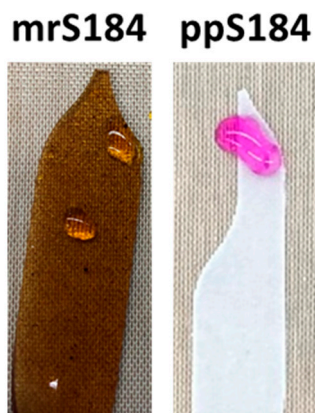


Figure 5. Surface sensing properties of mrS184 and ppS184. Observe that the sensors themselves did not change color but the clear liquid that was applied did.

When liquid phase tests were performed, color-changing droplets were observed in a similar fashion to mrS184 and ppS184 samples. Droplets on tbS184 changed from clear to dark blue, those on bbS184 became light blue, and those on apS184 and myS184 became red. Therefore, all of these composites demonstrate surface sensing properties as well.

3.2. Sensor Material Characterization

FTIR spectra for the composites revealed that the signal from Sylgard 184 overshadows the peaks from the indicators. This makes sense considering that the composites are between 90% and 99.5% Sylgard 184, meaning that the vibrational modes of the indicators barely contribute to the overall spectra. That stated, no new peaks were observed, demonstrating that no chemical interactions occurred between the indicators and Sylgard 184 and thus the FTIR spectra reveal that the sensors are true composites.

In addition to the sensing properties the indicators imbue to the composites, other characteristics and material properties of Sylgard 184 were affected as well. Because the lowest mass fraction of indicators (0.5 wt.%) worked well as composite sensors, the material properties were tested using these samples. As a starting point, the actual polymer network was investigated via solvent swelling in toluene. This allows for the evaluation of the network swelling and specific crosslink density using Equation (1). The densities of the 0.5 wt.% samples were approximately 1.06 g/cm^3 . As noted in previous literature, some mechanical properties correlate with the structure of the polymer network and its degree of crosslinking [56,58,59], thus the Shore A Hardness values for the samples are presented along with the network swelling values and specific crosslink densities for the sensors in Table 3. In general, solvent swelling is inversely related to the density of crosslinks in a network, so lower swelling values indicate that the crosslink density is greater. Reviewing Table 3, the values correspond to this relationship, where the largest network swelling values are from bpS184, apS184, mrS184, and myS184 (all above the network swelling value of 147% for Sylgard 184), which also exhibit the lowest specific crosslink density (all below $2.60 \times 10^{-4} \text{ mol crosslink/g material}$). Additionally, the least network swelling occurs in tbS184 (106%), which has the greatest specific crosslink density (almost $4 \times 10^{-4} \text{ mol crosslink/g material}$). Furthermore, a positively-correlated relationship between a material's specific crosslink density and resistance to indentation (Shore A Hardness) is observed in Table 3. Based on how the indicators affect the material properties, the hardest composites, ppS184, tpS184, tbS184, and bbS184 (all above 40 ShA and above $3 \times 10^{-4} \text{ mol crosslink/g material}$), can be classified as reinforcing fillers and the softest composites, myS184, bpS184, apS184, and mrS184 (all below 33 ShA), can be

classified as plasticizers [60,61]. Relevant data for regular Sylgard 184 is also included in Table 3.

Table 3. Solvent swelling properties and Shore A Hardness of the 0.5 wt.% composite chromophoric sensors compared to Sylgard 184.

Sample	Network Swelling (%)	Specific Crosslink Density (mol Crosslink/g Material)	Shore A Hardness
tpS184	115 ± 3	3.60×10^{-4}	42.6 ± 0.4
bpS184	151 ± 2	2.52×10^{-4}	31.2 ± 1.0
apS184	149 ± 7	2.57×10^{-4}	31.2 ± 1.4
tbS184	106 ± 0	3.94×10^{-4}	42.9 ± 0.2
bbS184	122 ± 2	3.35×10^{-4}	41.0 ± 1.1
ppS184	127 ± 2	3.27×10^{-4}	43.0 ± 0.4
mrS184	159 ± 3	2.44×10^{-4}	32.2 ± 0.6
myS184	149 ± 2	2.48×10^{-4}	30.4 ± 0.2
Sylgard 184	147 ± 1	3.16×10^{-4}	37.3 ± 0.3

Due to the polymer network being similar for all the composites, swelling data can be used to compare the polymer–indicator interactions. If an indicator interacts well with the polymer chains, there would be additional bonding, which could lead to an increase in specific crosslink density. Thus, indicators that behave as reinforcing fillers interact with the polymer network. Otherwise, the indicators do not interact well within the polymer network, leading to a plasticizing effect. This can aid in understanding the resulting structure and mechanical properties, especially when comparing the composites to regular Sylgard 184. Thus, for similar indicator concentrations, the composites with the greatest specific crosslink densities (tbS184, tpS184, bbS184, and ppS184) exhibit the best interactions with Sylgard 184. Swelling experiments support this argument, especially when evaluating the mass loss percent, which assesses the extracts. Although at 0.5 wt.% concentration the composites had similar losses of 4%, the extracts of composites with low specific crosslink densities (plasticizers) turned toluene from clear to a translucent but deep coloration. Indeed, apS184 and myS184 turned toluene yellow-orange and mrS184 turned toluene red. The only composite with a low specific crosslink density that did not change the color of toluene was bpS184, which did not exhibit any sensing properties. This phenomenon of toluene changing color did not occur with the composites exhibiting a higher specific crosslink density (reinforcing fillers). Furthermore, when solvent swelling experiments were performed on 10 wt.% sensors, the loss percent of the composites with good interactions remained at 4% while the composites with no interactions increased to 10%.

Understanding the applicable range of the sensors requires a knowledge of their thermal stability. Three measures of thermal stability allow for a broad understanding of their use, and they are the onset of thermal degradation Td5%, temperature of thermal decomposition TdMax, and residual mass mf. These thermal stability properties are given in Table 4. The composites fall within a 26 °C range for Td5% (400–426 °C), which shows an improvement of at least 30 °C compared to regular Sylgard 184 (a Td5% of 370 °C was demonstrated in our own laboratory results in and literature) [56,62,63]. The TdMax of the composites is more varied, where the range spans 266 °C (499–665 °C). These temperatures correspond to the breaking of the main PDMS chain backbone, which occurs from 400–650 °C [64–66]. In Sylgard 184 the largest thermal decomposition peak occurs around 540 °C in a nitrogen atmosphere, which resides within the range of PDMS backbone decomposition. The thermal decomposition of the sensors, like Sylgard 184, exhibit multiple decomposition peaks within the described range, and despite their maximal peaks varying with temperature they all fall within these bounds. Residual masses are lower than Sylgard 184, which exhibits a final mass percent between 40–50%. Thus, thermal decomposition releases more volatiles from the sensors than Sylgard 184.

Table 4. Thermal properties of the 0.5 wt.% composite chromophoric sensors compared to Sylgard 184.

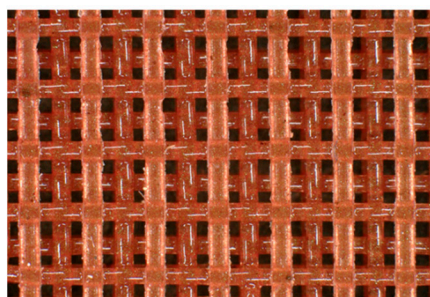
Sample	T _{d5%} (°C)	T _{dMax} (°C)	m _f (%)
tpS184	409	544	33
bpS184	424	616	46
apS184	400	508	31
tbS184	426	579	47
bbS184	415	665	31
ppS184	409	499	35
mrS184	423	527	20
myS184	408	527	28
Syglard 184	370	540	45

3.3. 3D Printing

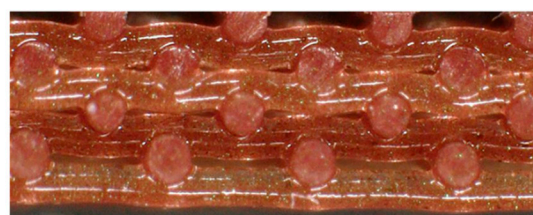
Pads with FCT structure described in previous work were successfully 3D printed using the formulation described in Section 2.2 (15 wt.% fumed silica) with low (0.5 and 1 wt.%) amounts of indicator (see Figure 6). A 3D printed FCT pad was also printed with 10 wt.% thermal paint to make the color change more discernable. Like the casted cylindrical samples, the 3D printed sensors were cured at 25 °C for two days. Additionally, some FCT pads were cured at 150 °C for two hours to investigate how accelerated curing would affect the composites. Interestingly, the only visible difference between these two curing procedures was with tbS184 and bbS184, both of which exhibited a color change. While the room temperature cured tbS184 FCT pad was dark green like the casted cylinder, the sample cured at an elevated temperature was a deep violet color. For the bbS184, the difference was a light pink hue when cured at an elevated temperature instead of a yellow-beige color when cured at room temperature. Although the bbS184 FCT pads had a low amount of indicator, the light pink hue was similar to a high weight percent loading bromothymol blue (which is a pink powder) as a casted cylinder (see Figure 1).

Face-Centered Tetragonal Structure

Top view



Side view

**Figure 6.** A 3D printed sensor with an FCT structure.

Further interesting observations were made concerning the tbS184, bbS184, and mrS184 FCT pads. The first is that despite the varying curing regimes producing different colored tbS184 and bbS184 parts, they still exhibited a halochromic sensing property, as seen in Figure 7. The second observation is that the mrS184 parts were able to be distinguishable when exposed to acidic species. Indeed, by having some porosity an observable color change occurred, where the 3D printed sensor transitioned from dark red to dark violet after exposure to either hydrochloric acid or nitric acid. Similarly, 3D printed tbS184 was more readily distinguishable once exposed to basic species than its casted counterpart. The other 3D printed sensors also behaved well as chromophoric devices. The increase in efficacy (being able to distinguish pristine and exposed tbS184 and mrS184) for the 3D printed sensors over the casted samples can be explained with an increase in surface area and porosity, which allows a greater amount of active sites and better visibility in

any color change. Thus, 3D printed DIW chromophoric sensors allow for a broader range of materials to be used where traditionally manufactured composites are difficult to be applicable in less than ideal situations such a low-light scenarios.

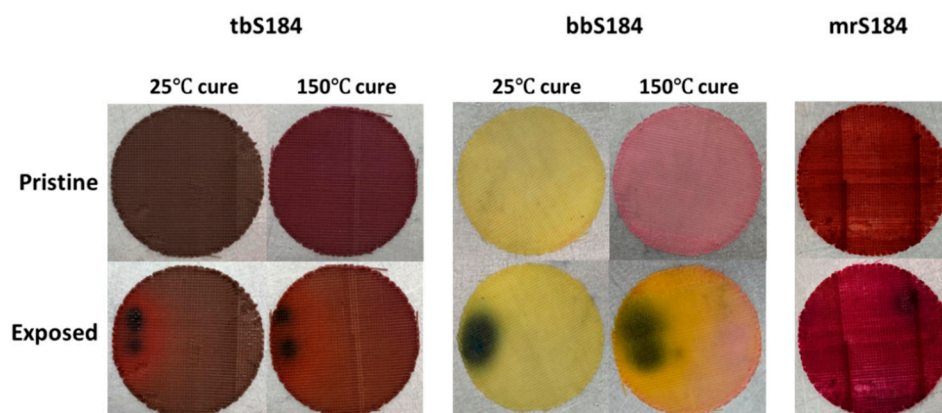


Figure 7. Comparison of the color changes in some of the 3D printed sensors—The sensors tb184 and bbS184 exhibited a color change when cured at an elevated temperature but it did not disrupt their sensing ability. Additionally, the porosity in the 3D printed sensors aided in providing a better visual cue for when tbS184 and mrS184 were exposed to basic or acidic chemical species, respectively.

4. Conclusions

Chromophoric sensors were developed as composite soft matter materials using Sylgard 184 and various indicators. Paint-based indicators were acid detecting paint, base detecting paint, and non-reversible single-change indicating thermal paint 155 °C. Powder-based indicators were thymol blue, bromothymol blue, phenolphthalein, methyl red, and methyl yellow. The sensors were fabricated using four different indicator proportions (0.5, 1, 5, and 10 wt.%) and it was found that if sensing properties were observable at all, they were observable for any of the four ratios investigated. Because of this ability for the sensors to successfully perform and change colors in the presence of stimuli, only 0.5 wt.% indicator is necessary for applications investigated in this work. For actual sensing properties, bpS184 did not exhibit any halochromic behavior, ppS184 exhibited only surface sensing halochromic behavior via vapor exposure, and all the other composites demonstrated not only surface sensing behavior, but could respond to vapor and liquid phase exposures. Although the tbS184 and mrS184 composites did change color once exposed, as evidenced by the UV-Vis experiments, the sensors fabricated using the traditional manufacturing technique were difficult to detect with the unaided eye. Once the sensing devices exhibited a color change, they remained in the exposed state without reverting. Additionally, the samples could be stored for at least a year and still perform as intended. Therefore, these composite chromophoric sensors are passive, irreversible, and possess a long lifespan, allowing them to demonstrate that a change in the immediate environment had occurred.

Probing the chemical structure of the composites revealed that no new chemical bonds were formed; therefore, the materials displayed additional properties to Sylgard 184. Additionally, solvent swelling experiments investigated the polymer network and demonstrated that tbS184, tpS184, bbS184, and ppS184 interacted well with Sylgard 184, forming additional crosslinks and increasing the mechanical properties while myS184, bpS184, apS184, and mrS184 did not interact with the polymer network. Thermal properties of the composites were evaluated as well, which demonstrated that the thermal stability and applicability of the sensors were similar.

The chromophoric sensors with 15 wt.% fumed silica were 3D printed using DIW and were cured at 25 °C for two days or 150 °C for two hours. Varying the temperatures demonstrated that the materials were able to perform as sensors at these two curing regimes. Additionally, composites that were difficult to distinguish between pristine and exposed via a traditional casting method (tbS184 and mrS184) were easier to discern as printed

sensors because of porosity. Thus, these passive environmental chromophoric sensors can be engineered into flexible, long-lasting customized shapes and fabricated using traditional or advanced manufacturing techniques, which easily scales up and is cost-efficient to do so.

Author Contributions: Z.B.: Conceptualization; data curation; formal analysis; investigation; methodology; project administration; resources; software; supervision; validation; visualization; writing—original draft; writing—review and editing. J.R.: Investigation; formal analysis; software; validation; writing—original draft; writing—review and editing. A.L.: Funding acquisition; project administration; resources; supervision; writing—review and editing. All authors have read and agreed to the published version of the manuscript.

Funding: This work was performed under the US Department of Energy’s National Nuclear Security Administration contract DE-AC52-06NA25396.

Data Availability Statement: The authors confirm that the data supporting the findings of this study are available within the article.

Acknowledgments: The authors would like to thank Josemari Sansiñena for his assistance in performing the UV-Vis spectroscopy experiments. Additionally, the authors gratefully acknowledge Campaign 2: Dynamic Materials Properties and the Radiation Shielding Program at Los Alamos National Laboratory for project support.

Conflicts of Interest: The authors declare no conflict of interest.

References

1. Jung, B.-J.; Kim, J.; Kim, J.-A.; Jang, H.; Seo, S.; Lee, W. PDMS-parylene hybrid, flexible microfluidics for real-time modulation of 3D helical inertial microfluidics. *Micromachines* **2018**, *9*, 255. [[CrossRef](#)] [[PubMed](#)]
2. Warkiani, M.E.; Khoo, B.L.; Tan, D.S.-W.; Bhagat, A.A.S.; Lim, W.-T.; Yap, Y.S.; Lee, S.C.; Soo, R.A.; Han, J.; Lim, C.T. An ultra-high-throughput spiral microfluidic biochip for the enrichment of circulating tumor cells. *Analyst* **2014**, *139*, 3245–3255. [[CrossRef](#)]
3. Bhagat, A.A.S.; Hou, H.W.; Li, L.D.; Lim, C.T.; Han, J. Pinched flow coupled shear-modulated inertial microfluidics for high-throughput rare blood cell separation. *Lab A Chip* **2011**, *11*, 1870–1878. [[CrossRef](#)]
4. Warkiani, M.E.; Bhagat, A.A.S.; Khoo, B.L.; Han, J.; Lim, C.T.; Gong, H.Q.; Fane, A.G. Isoporous Micro/Nanoengineered Membranes. *ACS Nano* **2013**, *7*, 1882–1904. [[CrossRef](#)] [[PubMed](#)]
5. Nam, J.; Jang, W.S.; Lim, C.S. Viscoelastic separation and concentration of fungi from blood for highly sensitive molecular diagnostics. *Sci. Rep.* **2019**, *9*, 1–12. [[CrossRef](#)]
6. Chun, J.; Kim, J.W.; Jung, W.-S.; Kang, C.-Y.; Kim, S.-W.; Wang, Z.L.; Baik, J.M. Mesoporous pores impregnated with Au nanoparticles as effective dielectrics for enhancing triboelectric nanogenerator performance in harsh environments. *Energy Environ. Sci.* **2015**, *8*, 3006–3012. [[CrossRef](#)]
7. Shahriar, M.; Vo, C.P.; Ahn, K.K. Self-powered flexible PDMS channel assisted discrete liquid column motion based triboelectric nanogenerator (DLC-TENG) as mechanical transducer. *Int. J. Precis. Eng. Manuf. Green Technol.* **2019**, *6*, 907–917. [[CrossRef](#)]
8. Zhu, G.; Yang, W.Q.; Zhang, T.; Jing, Q.; Chen, J.; Zhou, Y.S.; Bai, P.; Wang, Z.L. Self-powered, ultrasensitive, flexible tactile sensors based on contact electrification. *Nano Lett.* **2014**, *14*, 3208–3213. [[CrossRef](#)]
9. Shin, S.-Y.; Saravanakumar, B.; Ramadoss, A.; Kim, S.J. Fabrication of PDMS-based triboelectric nanogenerator for self-sustained power source application. *Int. J. Energy Res.* **2016**, *40*, 288–297. [[CrossRef](#)]
10. Borenstein, J.T.; Terai, H.; King, K.R.; Weinberg, E.; Kaazempur-Mofrad, M.; Vacanti, J. Microfabrication technology for vascularized tissue engineering. *Biomed. Microdevices* **2002**, *4*, 167–175. [[CrossRef](#)]
11. Leclerc, E.; Sakai, Y.; Fujii, T. A multi-layer PDMS microfluidic device for tissue engineering applications. In Proceedings of the Sixteenth Annual International Conference on Micro Electro Mechanical Systems, Kyoto, Japan, 23 January 2003; pp. 415–418.
12. Mata, A.; Fleischman, A.J.; Roy, S. Characterization of polydimethylsiloxane (PDMS) properties for biomedical micro/nanosystems. *Biomed. Microdevices* **2005**, *7*, 281–293. [[CrossRef](#)]
13. Li, J.; Liu, X.; Crook, J.; Wallace, G.G. Development of a porous 3D graphene-PDMS scaffold for improved osseointegration. *Colloids Surf. B Biointerfaces* **2017**, *159*, 386–393. [[CrossRef](#)]
14. Wang, C.C.; Ding, Z.; Purnawali, H.; Huang, W.M.; Fan, H.; Sun, L. Repeated Instant Self-healing Shape Memory Composites. *J. Mater. Eng. Perform.* **2012**, *21*, 2663–2669. [[CrossRef](#)]
15. Orellana, J.; Moreno-Villoslada, I.; Bose, R.K.; Picchioni, F.; Flores, M.E.; Araya-Hermosilla, R. Self-healing polymer nanocomposite materials by Joule effect. *Polymers* **2021**, *13*, 649. [[CrossRef](#)] [[PubMed](#)]
16. Sun, L.; Huang, W.; Ding, Z.; Zhao, Y.; Wang, C.; Purnawali, H.; Tang, C. Stimulus-responsive shape memory materials: A review. *Mater. Des.* **2012**, *33*, 577–640. [[CrossRef](#)]
17. Cui, H.P.; Song, C.L.; Huang, W.M.; Wang, C.C.; Zhao, Y. Rubber-like electrically conductive polymeric materials with shape memory. *Smart Mater. Struct.* **2013**, *22*, 055024. [[CrossRef](#)]

18. Murphy, E.; Dumont, J.H.; Park, C.H.; Kestell, G.; Lee, K.; Labouriau, A. Tailoring properties and processing of Sylgard 184: Curing time, adhesion, and water affinity. *J. Appl. Polym. Sci.* **2020**, *137*, 48530. [[CrossRef](#)]
19. Brounstein, Z.; Zhao, J.; Wheat, J.; Labouriau, A. Tuning the 3D Printability and Thermomechanical Properties of Radiation Shields. *Polymers* **2021**, *13*, 3284. [[CrossRef](#)] [[PubMed](#)]
20. Ibarlucea, B.; Fernández-Sánchez, C.; Demming, S.; Büttgenbach, S.; Llobera, A. Selective functionalisation of PDMS-based photonic lab on a chip for biosensing. *Analyst* **2011**, *136*, 3496–3502. [[CrossRef](#)]
21. Ghasemi, M.; Roostaei, N.; Sohrabi, F.; Hamidi, S.; Choudhury, P. Biosensing applications of all-dielectric SiO₂/PDMS meta-stadium grating nanocombs. *Opt. Mater. Express* **2020**, *10*, 1018–1033. [[CrossRef](#)]
22. Van Dang, B.; Hassanzadeh-Barforoushi, A.; Syed, M.S.; Yang, D.; Kim, S.-J.; Taylor, R.A.; Liu, G.-J.; Liu, G.; Barber, T. Microfluidic Actuation via 3D-Printed Molds toward Multiplex Biosensing of Cell Apoptosis. *ACS Sens.* **2019**, *4*, 2181–2189. [[CrossRef](#)]
23. Su, L.; Jiang, Z.; Tian, Z.; Wang, H.; Wang, H.; Zi, Y. Self-powered, ultrasensitive, and high-resolution visualized flexible pressure sensor based on color-tunable triboelectrification-induced electroluminescence. *Nano Energy* **2021**, *79*, 105431. [[CrossRef](#)]
24. Lei, K.F.; Lee, K.-F.; Lee, M.-Y. Development of a flexible PDMS capacitive pressure sensor for plantar pressure measurement. *Microelectron. Eng.* **2012**, *99*, 1–5. [[CrossRef](#)]
25. Gong, X.X.; Fei, G.T.; Fu, W.B.; Fang, M.; Gao, X.D.; Zhong, B.N.; De Zhang, L. Flexible strain sensor with high performance based on PANI/PDMS films. *Org. Electron.* **2017**, *47*, 51–56. [[CrossRef](#)]
26. Wu, S.; Ladani, R.B.; Zhang, J.; Ghorbani, K.; Zhang, X.; Mouritz, A.P.; Kinloch, A.J.; Wang, C.H. Strain Sensors with Adjustable Sensitivity by Tailoring the Microstructure of Graphene Aerogel/PDMS Nanocomposites. *ACS Appl. Mater. Interfaces* **2016**, *8*, 24853–24861. [[CrossRef](#)] [[PubMed](#)]
27. Yang, J.; Wei, D.; Tang, L.; Song, X.; Luo, W.; Chu, J.; Gao, T.; Shi, H.; Du, C. Wearable temperature sensor based on graphene nanowalls. *RSC Adv.* **2015**, *5*, 25609–25615. [[CrossRef](#)]
28. Wu, L.; Qian, J.; Peng, J.; Wang, K.; Liu, Z.; Ma, T.; Zhou, Y.; Wang, G.; Ye, S. Screen-printed flexible temperature sensor based on FG/CNT/PDMS composite with constant TCR. *J. Mater. Sci. Mater. Electron.* **2019**, *30*, 9593–9601. [[CrossRef](#)]
29. Dang, W.; Manjakkal, L.; Lorenzelli, L.; Vinciguerra, V.; Dahiya, R. Stretchable pH sensing patch in a hybrid package. In Proceedings of the 2017 IEEE SENSORS, Glasgow, UK, 29 October–1 November 2017; IEEE: New York, NY, USA, 2017; pp. 1–3.
30. Sousa, R.P.C.L.; Ferreira, B.; Azenha, M.; Costa, S.P.G.; Silva, C.J.R.; Figueira, R. PDMS Based Hybrid Sol-Gel Materials for Sensing Applications in Alkaline Environments: Synthesis and Characterization. *Polymers* **2020**, *12*, 371. [[CrossRef](#)]
31. Mani, G.K.; Nimura, Y.; Tsuchiya, K. Advanced Artificial Electronic Skin Based pH Sensing System for Heatstroke Detection. *ACS Sens.* **2020**, *5*, 911–916. [[CrossRef](#)]
32. Komazaki, Y.; Uemura, S. Stretchable, printable, and tunable PDMS-CaCl₂ microcomposite for capacitive humidity sensors on textiles. *Sens. Actuators B Chem.* **2019**, *297*, 126711. [[CrossRef](#)]
33. Tripathy, A.; Sharma, P.; Sahoo, N.; Pramanik, S.; Abu Osman, N. Moisture sensitive inimitable Armalcolite/PDMS flexible sensor: A new entry. *Sens. Actuators B Chem.* **2018**, *262*, 211–220. [[CrossRef](#)]
34. Hwang, I.-S.; Kim, Y.-S.; Kim, S.-J.; Ju, B.-K.; Lee, J.-H. A facile fabrication of semiconductor nanowires gas sensor using PDMS patterning and solution deposition. *Sens. Actuators B Chem.* **2009**, *136*, 224–229. [[CrossRef](#)]
35. Nam, Y.-S.; Yoo, I.; Yarimaga, O.; Park, I.S.; Park, D.-H.; Song, S.; Kim, J.-M.; Lee, C.W. Photochromic spiropyran-embedded PDMS for highly sensitive and tunable optochemical gas sensing. *Chem. Commun.* **2014**, *50*, 4251–4254. [[CrossRef](#)]
36. Zhang, H.; Byrne, R. Spectrophotometric pH measurements of surface seawater at in-situ conditions: Absorbance and protonation behavior of thymol blue. *Mar. Chem.* **1996**, *52*, 17–25. [[CrossRef](#)]
37. Yamazaki, H.; Sperline, R.; Freiser, H. Spectrophotometric determination of the dissociation constant (pK_a) of arsenous acid. *Anal. Chim. Acta* **1993**, *284*, 379–384. [[CrossRef](#)]
38. Balderas, P.; Ramírez-Silva, M.T.; Romo, M.A.R.; Palomar-Pardavé, M.; Roa, G.; Barrera-Díaz, C.E.; Rojas-Hernández, A. Experimental correlation between the pK_a value of sulfonphthaleins with the nature of the substituents groups. *Spectrochim. Acta Part A Mol. Biomol. Spectrosc.* **2008**, *69*, 1235–1245. [[CrossRef](#)]
39. Zaggout, F.R.; El-Nahhal, I.M.; Qaraman, A.E.-F.A.; Al Dahoudi, N. Behavior of thymol blue analytical pH-indicator entrapped into sol-gel matrix. *Mater. Lett.* **2006**, *60*, 3463–3467. [[CrossRef](#)]
40. Nakamura, N.; Amao, Y. An optical sensor for CO₂ using thymol blue and europium(III) complex composite film. *Sens. Actuators B Chem.* **2003**, *92*, 98–101. [[CrossRef](#)]
41. Nakamura, N.; Amao, Y. Optical sensor for carbon dioxide combining colorimetric change of a pH indicator and a reference luminescent dye. *Anal. Bioanal. Chem.* **2003**, *376*, 642–646. [[CrossRef](#)]
42. Stocker, M.K.; Sanson, M.L.; Bernardes, A.A.; Netto, A.M.; Brambilla, R. Acid-base sensor based on sol-gel encapsulation of bromothymol blue in silica: Application for milk spoilage detection. *J. Sol.-Gel. Sci. Technol.* **2021**, *98*, 568–579. [[CrossRef](#)]
43. Pradhan, P.; Mascarenhas, R.J.; Thomas, T.; Namboothiri, I.N.; D'Souza, O.J.; Mekhalif, Z. Electropolymerization of bromothymol blue on carbon paste electrode bulk modified with oxidized multiwall carbon nanotubes and its application in amperometric sensing of epinephrine in pharmaceutical and biological samples. *J. Electroanal. Chem.* **2014**, *732*, 30–37. [[CrossRef](#)]
44. Liu, Z.; Luo, F.; Chen, T. Phenolphthalein immobilized membrane for an optical pH sensor. *Anal. Chim. Acta* **2004**, *510*, 189–194. [[CrossRef](#)]
45. Sharifabad, A.N.; Bahrami, S.H. Halochromic chemosensor from poly (acrylonitrile)/phenolphthalein nanofibers as pH sensor. *IEEE Sens. J.* **2015**, *16*, 873–880. [[CrossRef](#)]

46. Ali, S.; Hassan, A.; Hassan, G.; Bae, J.; Lee, C.H. All-printed humidity sensor based on graphene/methyl-red composite with high sensitivity. *Carbon* **2016**, *105*, 23–32. [[CrossRef](#)]
47. Hassan, G.; Sajid, M.; Choi, C. Highly Sensitive and Full Range Detectable Humidity Sensor using PEDOT:PSS, Methyl Red and Graphene Oxide Materials. *Sci. Rep.* **2019**, *9*, 1–10. [[CrossRef](#)]
48. Singh, G.; Girdhar, S.; Singh, A.; Saroa, A.; Lakhi, J.S.; Khullar, S.; Mandal, S.K. Selective mercury ion recognition using a methyl red (MR) based silatrane sensor. *New J. Chem.* **2018**, *42*, 6315–6321. [[CrossRef](#)]
49. Nakano, N.; Ishikawa, M.; Kobayashi, Y.; Nagashima, K. Development of a Monitoring Tape for Formaldehyde Using Hydroxylamine Sulfate and Methyl Yellow. *Anal. Sci.* **1994**, *10*, 641–645. [[CrossRef](#)]
50. Wang, X.; Si, Y.; Wang, J.; Ding, B.; Yu, J.; Al-Deyab, S.S. A facile and highly sensitive colorimetric sensor for the detection of formaldehyde based on electro-spinning/netting nano-fiber/nets. *Sens. Actuators B Chem.* **2012**, *163*, 186–193. [[CrossRef](#)]
51. Cruickshank, D.L.; Hendon, C.H.; Verbeek, M.J.R.; Walsh, A.; Wilson, C.C. Polymorphism of the azobenzene dye compound methyl yellow. *CrystEngComm* **2016**, *18*, 3456–3461. [[CrossRef](#)]
52. Patterson, G.S. A Simplified Method for Finding the pKa of an Acid-Base Indicator by Spectrophotometry. *J. Chem. Educ.* **1999**, *76*, 395. [[CrossRef](#)]
53. Shokrollahi, A.; Zarghampour, F.; Akbari, S.; Salehi, A. Solution scanometry, a new method for determination of acidity constants of indicators. *Anal. Methods* **2015**, *7*, 3551–3558. [[CrossRef](#)]
54. Chasse, W.; Lang, M.; Sommer, J.-U.; Saalwächter, K. Cross-link density estimation of PDMS networks with precise consideration of networks defects. *Macromolecules* **2012**, *45*, 899–912. [[CrossRef](#)]
55. Dimitriyev, M.S.; Chang, Y.-W.; Goldbart, P.M.; Fernández-Nieves, A. Swelling thermodynamics and phase transitions of polymer gels. *Nano Futures* **2019**, *3*, 042001. [[CrossRef](#)]
56. Brounstein, Z.; Zhao, J.; Geller, D.; Gupta, N.; Labouriau, A. Long-Term Thermal Aging of Modified Sylgard 184 Formulations. *Polymers* **2021**, *13*, 3125. [[CrossRef](#)]
57. Chassé, W.; Lang, M.; Sommer, J.-U.; Saalwächter, K. Correction to cross-link density estimation of PDMS networks with precise consideration of networks defects. *Macromolecules* **2015**, *48*, 1267–1268. [[CrossRef](#)]
58. Krumova, M.; López, D.; Benavente, R.; Mijangos, C.; Pereña, J. Effect of crosslinking on the mechanical and thermal properties of poly(vinyl alcohol). *Polymers* **2000**, *41*, 9265–9272. [[CrossRef](#)]
59. Safranski, D.L.; Gall, K. Effect of chemical structure and crosslinking density on the thermo-mechanical properties and toughness of (meth)acrylate shape memory polymer networks. *Polymers* **2008**, *49*, 4446–4455. [[CrossRef](#)]
60. Dumont, J.; Murphy, E.; Geller, D.; Lee, K.-S.; Labouriau, A. Effects of thermal aging and ionizing radiation on sPVC and aromatic polyether urethane used to store nuclear materials. *Polym. Test.* **2019**, *78*, 105960. [[CrossRef](#)]
61. Titow, M. *PVC Technology*; Springer Science & Business Media: Berlin, Germany, 2012.
62. Engel, J.; Chen, J.; Bullen, D.; Liu, C. Polyurethane rubber as a MEMS material: Characterization and demonstration of an all-polymer two-axis artificial hair cell flow sensor. In Proceedings of the 18th IEEE International Conference on Micro Electro Mechanical Systems, Miami Beach, FL, USA, 30 January–3 February 2005; IEEE: New York, NY, USA, 2005; pp. 279–282.
63. Zulfiqar, S.; Ahmad, S. Thermal degradation of blends of PVAC with polysiloxane—II. *Polym. Degrad. Stab.* **2001**, *71*, 299–304. [[CrossRef](#)]
64. Olima, M. Mechanical Characterization of Polydimethylsiloxane. Master's Thesis, The University of Oklahoma, Norman, OK, USA, 2017.
65. Thomas, T.H.; Kendrick, T.C. Thermal analysis of polydimethylsiloxanes. I. Thermal degradation in controlled atmospheres. *J. Polym. Sci. Part A-2 Polym. Phys.* **1969**, *7*, 537–549. [[CrossRef](#)]
66. Örn, A. Degradation Studies on Polydimethylsiloxane. Master's Thesis, Åbo Akademi University, Turku, Finland, 2019.